CrystEngComm

Flux-assisted Polytypism in the [Na2Cl]GaQ2 Heterolayered Salt-Inclusion Chalcogenide Family

Journal:	*CrystEngComm*
Manuscript ID	CE-ART-01-2023-000074.R1
Article Type:	Paper
Date Submitted by the Author:	13-Mar-2023
Complete List of Authors:	Berseneva, Anna; University of South Carolina, Department of Chemistry and Biochemistry Klepov, Vladislav; University of Georgia Tisdale, Hunter; University of South Carolina Zur Loye, Hans-Conrad; University of South Carolina, Department of Chemistry and Biochemistry

Flux-assisted Polytypism in the $[Na_2Cl]GaQ_2$ Heterolayered Salt-Inclusion Chalcogenide Family

Anna A. Berseneva,[a] Vladislav V. Klepov,[b] Hunter B. Tisdale,[a] Hans-Conrad zur Loye[a]*

[a] Department of Chemistry and Biochemistry, University of South Carolina, Columbia, South Carolina, 29208, USA

[b] Department of Chemistry, University of Georgia, Athens, Georgia, 30602, USA

*Corresponding author. E-mail: zurloye@mailbox.sc.edu

ABSTRACT: Two polytypic heterolayered salt-inclusion chalcogenides, *o*-[Na_2Cl]GaQ_2 and *t*-[Na_2Cl]GaQ_2, were obtained *via* a NaCl/NaI *flux-assisted synthesis,* as part of an investigation of the Na–Ga–*Q* (*Q* = S and Se) system. The use of a different flux, NaBr/NaI, in the Na–Ga–Se system did not led to the formation of salt-inclution phases, but instead the novel Na_2GaSe_3 and $Na_4Ga_2Se_5$ phases were obtained. Thermal and electronic properties of [Na_2Cl]GaS_2 materials were investigated with differential scanning calorimetry, post-quenching *ex situ* powder X-ray diffraction (PXRD), high-temperature PXRD, and enthalpy and electronic structure calculations *via* density functional theory. Those studies determined the absence of any temperature-induced phase transition between the *o*-[Na_2Cl]GaS_2 and *t*-[Na_2Cl]GaS_2 polytypic compounds. Moreover, we probed the suitability of the heterolayered [Na_2Cl]GaS_2 single crystals as a sorbent for UO_2^{2+} uptake and monitored this process by energy-dispersive and infrared spectroscopies and PXRD, which revealed that the $[Na_2Cl]^+$ insert could be exchanged with UO_2^{2+} on the surface while the UO_2^{2+} intercalation decomposes the [Na_2Cl]GaS_2 structure.

Hybrid materials consist of two or more building blocks that assemble to form structures that can, at times, exhibit desirable properties due to the simultaneous presence of different unique building units. In fact, hybrid materials have demonstrated outstanding potential for applications which include energy harvesting, solid-state lighting, and semiconductor technology.[1–9] Unsurprising, the field is dominated by organic-inorganic hybrid structures that include lead halide perovskites[10–13] and metal-organic frameworks.[14–17] Another hybrid material class is the inorganic-inorganic hybrids, which are much less studied.[18–21] An example of an inorganic-inorganic hybrid is a salt inclusion material (SIM), which contains both a covalent and an ionic building block. While numerous SIMs are known that consist of an oxide framework and a salt inclusion, far fewer chalcogenide SIMs have been reported. In the latter case, the salt-inclusion hybrid structure consists of a covalent chalcogenide MQ_n framework (M = *p*-, *d*-, or *f*-metal) that coexists with an ionic salt component, typically consisting of a XA_m polyhedra (X = halogen and A = alkali and alkaline earth metals).[22–29] The covalent and ionic building blocks can have different functionalities that can potentially be tuned through framework or salt structure modifications.

Similar to organic-inorganic hybrid structures, salt-inclusion materials can also be classified based on the framework's dimensionality, but they can also be divided by the salt-inclusion fragment's dimensionality; both can vary from 0D to 3D. For example, the zur Loye group reported the structure of $[Cs_{13}Cl_5](UO_2)_3Al_2O(PO_4)_6$ that contains a porous 3D uranyl aluminophosphate framework 'stuffed' with a 3D cesium chloride-based salt-inclusion.[30] Another example is the $[Cs_6X]AGa_6Q_{12}$ family consisting of 0D Cs_6X and 2D gallium chalcogenide units.[31] Heterolayered compositions are structurally similar to salt-inclusion materials, as separate layers may be constructed from cation- and anion-centered polyhedra. For example, in $[M\text{O}]\text{Cu}Q$ (M = Bi and La; Q = S, Se, and Te), where the layered slabs consist of $\text{O}M_4$ and $\text{Cu}Q_4$ tetrahedra.[32] Importantly, 2D-2D salt-inclusion materials can be considered heterolayered structures, and while the synthesis of oxide-chalcogenide heterolayered compositions is challenging,[33,34] synthetic routes for salt-inclusion materials are more straightforward and can be achieved by adding salt to polychalcogenide flux. Herein, we report two polymorphs of salt-inclusion heterolayered compositions $[Na_2Cl]GaQ_2$ (Q = S and Se) obtained during the exploratory crystal growth in the Na–Ga–Q–NaCl system.

Using flux crystal growth, colorless square-block-like crystals of $[Na_2Cl]GaS_2$ were obtained in a reaction between Ga, S, Na_2S, NaCl, and NaI (see an experimental section for more details). We discovered that $[Na_2Cl]GaS_2$ can crystallize in two polymorphic modifications: the reported orthorhombic *o*-$[Na_2Cl]GaS_2$ (space group, sp. gr., *Cmcm*)[35] and the novel tetragonal *t*-$[Na_2Cl]GaS_2$ (sp. gr. $P4_2/nmc$), which differ in the GaS_2^- layer arrangement (Figures 1 and S1–S4 and Tables S1–S2). Using a similar synthesis procedure, we were able to substitute Se for S and obtained two additional polymorphs: *o*-$[Na_2Cl_{0.9}I_{0.1}]GaSe_2$ and *t*-$[Na_2Cl_{0.9}I_{0.1}]GaSe_2$ which are isostructural to the sulfide analogs. Due to the softer selenide compared to the sulfide anion, the selenide analogs contain iodide in addition to chloride on the halogen site resulting in *o*-$[Na_2Cl_{0.9}I_{0.1}]GaSe_2$ and *t*-$[Na_2Cl_{0.9}I_{0.1}]GaSe_2$, as confirmed by single crystal X-ray diffraction (SC-XRD) and energy-dispersive spectroscopy (EDS, Figures S5–S8 and Table S3). The attempted

substitution of Na by other alkali metals (Li, K, Rb, and Cs) and of Cl by Br or I did not result in the formation of the salt-inclusion material but rather led to the formation of the known AGaS$_2$ phases (A = Li, K, Rb, and Cs) and, when a NaBr/NaI flux is used, to two novel selenide phases, Na$_2$GaSe$_3$ and Na$_4$Ga$_2$Se$_5$ (see ESI for more information, Figures S9–S11 and Table S4). Previously, the *o*-[Na$_2$Cl]GaS$_2$ structure was obtained by Li et al. using Ga$_2$S$_3$, Na$_2$S$_3$, and NaCl; however, the formation of a tetragonal polymorph was not mentioned.[35] It is possible that our use of NaI in the reaction mixture promoted the formation of the tetragonal polymorph. Moreover, Li reported that the reaction between Ga$_2$S$_3$, Na$_2$Se, and NaCl/NaBr reagents led to the formation of the known NaGa$_3$Se$_5$[35] rather than the salt-inclusion material, highlighting the significance of the role and impact of the flux on the formation of [Na$_2$Cl]GaQ_2 structures.

Both *t*-[Na$_2$Cl]GaQ_2 (Figure 1c) and *o*-[Na$_2$Cl]GaQ_2 (Figure 1e) are heterolayered structures which are comprised of a 2D gallium chalcogenide slabs (Figure 1a) separated by 2D salt-inclusion layers (Figure 1b). The building block of the ionic layer is the ClNa$_6$ trigonal prism (Figure 1b). The structure of the GaQ_2^- layers is similar to the one observed in the NaGaS$_2$ structure (KInS$_2$ structure type, Figure S12),[36] i.e., GaQ_2^- layers consisting of Ga$_4$S$_{10}$ supertetrahedral T$_2$ clusters that are connected through corner-sharing to create a square-net topology (Figure 1a). While the *o*-[Na$_2$Cl]GaQ_2 and *t*-[Na$_2$Cl]GaQ_2 structures have identical 2D gallium chalcogenide slabs and salt-inclusion layers (Table S2), they differ in the stacking arrangement of the GaQ_2^- layers. In the case of *t*-[Na$_2$Cl]GaQ_2 structure, there are two unique layers, A and B, where each successive layer is shifted by a/2 and b/2 relative to the preceding one (Figure 1d). While the *t*-[Na$_2$Cl]GaQ_2 structure exhibits an AB layer stacking sequence, the *o*-[Na$_2$Cl]GaQ_2 material is built up from four unique GaQ_2^- layers (Figure 1f), resulting in the doubling of the lattice parameter in comparison to the *t*-[Na$_2$Cl]GaQ_2 structure, i.e., 39.4434(10) Å vs. 19.7163(5) Å for sulfides. In the *o*-[Na$_2$Cl]GaQ_2 structure, the first two-layer stacking is identical to the *t*-[Na$_2$Cl]GaQ_2 composition, i.e., AB (Figures 1d and 1f). However, the C layer is shifted by a/2 relative to the B layer. The D layer is shifted half diagonal (a/2 and c/2) to the previous one, as in the AB stacking, and, finally, the A layer is shifted by c/2 relative to the D layer, as in the BC stacking (Figure 1f).

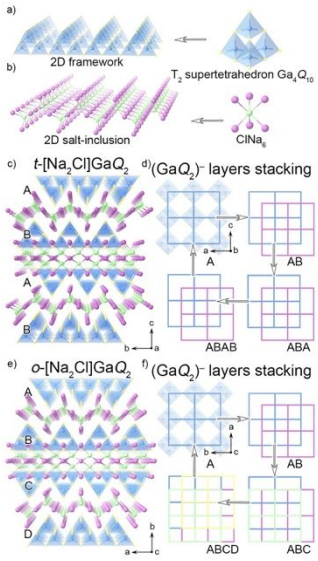

Figure 1. View of (*a*) the framework slabs and (b) the salt inclusion layer and the corresponding building blocks. Purple, green, blue, and yellow spheres and blue tetrahedra represent Na, Cl, Ga, and *Q* atoms and GaQ_4 polyhedra, respectively. View of (*c*) *t*-[Na_2Cl]GaS_2 and (*e*) *o*-[Na_2Cl]GaS_2. Stacking of T_2-corner-sharing layers in (*d*) *t*-[Na_2Cl]GaS_2 and (*f*) *o*-[Na_2Cl]GaS_2. Blue, purple, green, and yellow square-net present unique T_n-corner-sharing layers where a node is a T_2 supertetrahedral cluster.

After optimizing the synthetic procedure (see ESI for more information), we obtained phase pure samples of [Na_2Cl]GaQ_2 (Figures S13–S16). To identify any possible phase transition between the two polymorphs, we studied their thermal behavior using differential scanning calorimetry (DSC) coupled with thermogravimetric analysis (TGA) under an N_2 atmosphere (Figure S17). The DSC analysis demonstrated an irreversible event for [Na_2Cl]GaS_2 in the 570–580 °C temperature range that did not correspond to a polymorphic transformation (Figure S18). Overall, the sample is stable up to 720 °C under an N_2 atmosphere and, at higher temperatures, starts to decompose and oxidize in the presence of trace oxygen, as indicated by the weight loss on the TGA plot (Figure S19). Conversely, a vacuum-sealed single crystal sample of [Na_2Cl]GaS_2 was annealed and quenched at different temperatures, followed by *ex situ* PXRD analysis that demonstrated the decomposition of [Na_2Cl]GaS_2 to $NaGaS_2$ (which further transforms to $NaGaS_2 \cdot H_2O$ in the presence of air) and NaCl above 550 °C (Figure S20). High-temperature PXRD was performed on a [Na_2Cl]GaS_2 sample sealed in a capillary over the 100–650 °C temperature range and did not reveal any conversion between the two polymorphs, *o*-[Na_2Cl]GaS_2 and *t*-[Na_2Cl]GaS_2, at these temperatures (Figure S21). Hence we conclude that under thermal treatment, no phase transition takes place between the *o*-[Na_2Cl]GaS_2 and *t*-[Na_2Cl]GaS_2 polymorphs.

To shed light on the stability of the different polymorphs discussed herein, we turned to density functional theory (DFT) calculations. We estimated the enthalpies of formation at 0K, ΔH_f^{0K}, for the orthorhombic and the tetragonal polymorphs of [Na_2Cl]GaS_2.[37,38] Our calculations demonstrated that ΔH_f^{0K} are similar for the two compositions, –1.41589 eV/atom and –1.41586

eV/atom for *o*-$[Na_2Cl]GaS_2$ and *t*-$[Na_2Cl]GaS_2$, respectively (Table S5). This result helps to explain why we observed the formation of both polymorphs in the reaction mixture and why we could not isolate solely the orthorhombic or the tetragonal polymorph by performing the synthesis at different temperatures. DFT calculations also allow us to corroborate the decomposition pathway[37,38] that we noticed in our *ex situ* PXRD quenching experiments. The convex hull in the Na–Ga–S–Cl landscape for both *o*-$[Na_2Cl]GaS_2$ and *t*-$[Na_2Cl]GaS_2$ polymorphs estimates that decomposition leads to $NaGaS_2$ and NaCl with a positive ΔH_{decom}^{0K}, confirming the stability of both polymorphs. Using *t*-$[Na_2Cl]GaS_2$ as a model, we also estimated ΔH_{decom}^{0K} for the *t*-$[A_2X]GaS_2$ structures where *A* = Li, Na, and K and *X* = F, Cl, and Br (Figure 2) in the Reaction 1:

$$[A_2X]GaS_2 \rightarrow AGaQS_2 + AX \qquad \text{(Reaction 1)}$$

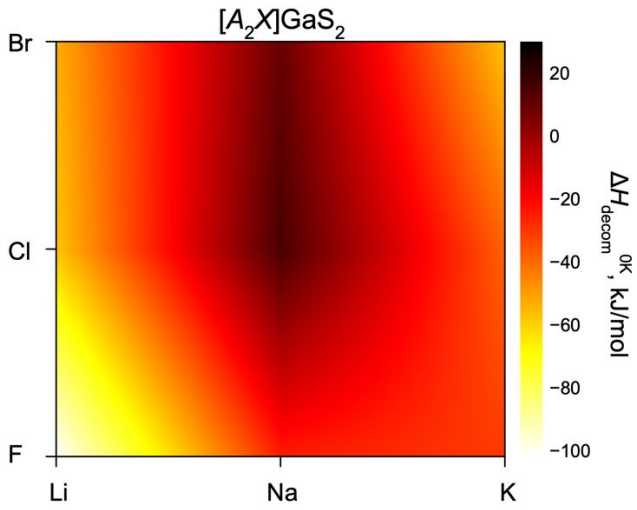

Figure 2. Contour plot of enthalpies of $[A_2X]GaS_2$ decomposition reactions leading to $AGaS_2$ and *AX*, as a function of *A* and *X*.[37,38] Note: only $[Na_2Cl]GaS_2$ was obtained synthetically.

A fast stability screening demonstrated a positive ΔH_{decom}^{0K} of 15.8 kJ/mol and 10.0 kJ/mol for *t*-$[Na_2Cl]GaS_2$ and *t*-$[Na_2Br]GaS_2$, respectively (Table S5). We were not able to obtain the $[Na_2Br]GaS_2$ analog; changing NaCl to NaBr in the synthesis resulted in the formation of $NaGaS_2$. Moreover, we probed ion-exchange reactions that previously demonstrated strong potential as being one synthetic approach for obtaining new compositions of 0D salt-inclusion materials that cannot be prepared directly;[31] however, our attempts to synthesize $[Na_2Br]GaS_2$ (see ESI for more information) using this approach did not succeed. In summary, the *t*-$[Na_2Cl]GaS_2$ composition is the most stable of the *t*-$[A_2X]GaS_2$ (*A* = Li, Na, and K; *X* = F, Cl, and Br) compositions based on their decomposition enthalpies (Figure 2 and Table S5).

To understand how structural differences affect the electronic structures of the *o*-$[Na_2Cl]GaS_2$ and the *t*-$[Na_2Cl]GaS_2$ polymorphs, we calculated the density of states (DOS) for these materials (Figure 3). The DOS analysis indicates an analogous electronic structure for both polymorphs, which is not surprising considering that their structures are based on the same

covalent part, the GaS_2^- layer. In both *o*-$[Na_2Cl]GaS_2$ and *t*-$[Na_2Cl]GaS_2$ compositions, the valence band is formed by S orbitals, while S and Ga orbitals form the conduction band. In other words, the electronic structure mainly depends on the GaS_2^- layers; this was also demonstrated for $NaGaS_2$ and $NaGaS_2 \cdot H_2O$,[39,40]and hence the specific stacking sequence of the GaS_2^- layers only minimally alters the electronic structure. Furthermore, using the Tauc plot derived from UV-Vis spectroscopy, we estimated the direct band gap for the $[Na_2Cl]GaS_2$ sample to be 3.99 eV (Figure S22), which agrees well with the lack of color in the crystals of *o*-$[Na_2Cl]GaS_2$ and *t*-$[Na_2Cl]GaS_2$. Previously, the band gaps for $NaGaS_2$ and $NaGaS_2 \cdot H_2O$ were estimated to be 3.95 eV and 4.00 eV, respectively,[39,40] confirming that optical properties are dominated by the GaS_2^- layers.

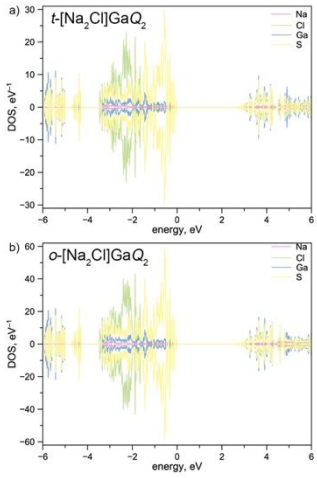

Figure 3. DOS of (*a*) *t*-$[Na_2Cl]GaS_2$ and (*c*) *o*-$[Na_2Cl]GaS_2$.

Previously, we reported that the layered $NaGaS_2$ can ion exchange 3*d* metal cations and UO_2^{2+}.[40] In general, layered chalcogenide materials are known to be excellent sorbents for uranyl species due to effective $UO_2^{2+} \cdots S^{2-}$ bonding interactions.[41–44] Therefore, we probed the ion-exchange properties of the salt-inclusion layered chalcogenides. For the ion exchange experiments, we used single crystals of $[Na_2Cl]GaS_2$ materials and soaked them in uranyl nitrate solutions of different concentrations, ranging from 0.001 M to 0.01 M (see ESI for more information). To assess the presence of UO_2^{2+} in the final product, we confirmed the appearance of a U–O stretch around 890–910 cm^{-1} in the infrared (IR) spectrum (Figure S23). Furthermore, the uranyl sorption was monitored by EDS (Figures 4 and S24–S26), and we probed the sample's crystallinity *via* PXRD (Figures S28 and S29). After 3 hours of uranyl-uptake with $[Na_2Cl]GaS_2$ single crystals, we noticed uranium adsorption only on the crystal surface, as shown for a cleaved crystal (Figures 4a, S24, and S25). The uranium uptake correlates with a decrease in the Na and Cl concentration (Figure 4a and Table S6). The salt-inclusion could be entirely exchanged with UO_2^{2+} after 24 hours of soaking in 0.01 M solutions (Figures 4b, 4c, and S26); however, it was accompanied by a loss of crystallinity, i.e., structure decomposition, as demonstrated by SEM and PXRD (Figures 4b, S26, and S27). As shown by the diffraction analysis of $[Na_2Cl]GaS_2$ that was soaked for 24 hours in 0.001–0.005 M UO_2^{2+} solutions (Figure S28), there is no shift in the position of the peaks that

reflect the interlayer separation, implying that uranyl does not intercalate between the GaS_2^- layers. On the other hand, there is an intensity reduction for peaks that do not correspond to the [0*k*0]- or [hk0]-family (*o*-$[Na_2Cl]GaS_2$ or *t*-$[Na_2Cl]GaS_2$, respectively) (Figure S28). At lower uranyl concentrations, the crystallinity of $[Na_2Cl]GaS_2$ is preserved when the uranium deposits on the crystal surface. At higher UO_2^{2+} concentrations (0.01 M), uranyl uptake is accompanied by a reduction in crystallinity as shown by PXRD (Figure S29) and complete leaching of Na^+ and Cl^- ions (Figures 4b and 4c), resulting in total loss of crystallinity and structure decomposition since uranyl species do not intercalate between the GaS_2^- layers to stabilize the structure.

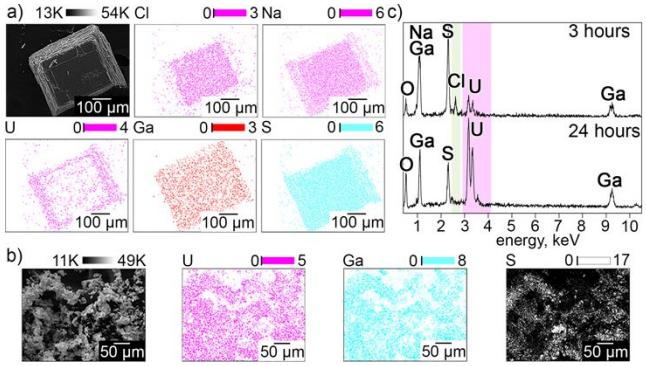

Figure 4. (*a*,*b*) EDS mapping and (*c*) EDS spectra of the $[Na_2Cl]GaS_2$ sample soaked in 0.01 M UO_2^{2+} solution for (*a*) 3 hours and (*b*) 24 hours. Pink and green boxes highlight U and Cl peak positions on EDS spectra, respectively.

In summary, we explored the role of the flux in assisting in the formation of new compositions and also in the formation of polymorphs. This approach resulted in the discovery of three novel structures of salt-inclusion materials, *t*-$[Na_2Cl]GaS_2$, *o*-$[Na_2Cl_{0.9}I_{0.1}]GaSe_2$, and *t*-$[Na_2Cl_{0.9}I_{0.1}]GaSe_2$, and two new sodium gallium selenides, Na_2GaSe_3 and $Na_4Ga_2Se_5$. These results suggest that exploring different fluxes for a given system can lead to discovering new materials.

To understand the stability of the *o*-$[Na_2Cl]Ga\mathit{Q}_2$ and *t*-$[Na_2Cl]Ga\mathit{Q}_2$ polymorphs, we performed DFT calculations to determine the enthalpy of formation, which demonstrated that the polymorphs have negligibly different formation energies. This result can explain the synthetic challenge of isolating only one of the two polymorphs, a process we studied *via ex situ* PXRD and HT-PXRD. The fast screening of stability was used as a tool to explore the compositional diversity of the *t*-$[\mathit{A}_2\mathit{X}]GaS_2$ (*A* = Li, Na, and K; *X* = F, Cl, and Br) family, showing that *t*-$[Na_2\mathit{X}]GaS_2$ (*X* = Cl and Br) are the most stable and that, as demonstrated by *ex situ* PXRD annealing experiments, all compositions decompose at elevated temperatures to $\mathit{A}GaS_2$ and *AX*. While the stability of the layered salt-inclusion materials *t*-$[\mathit{A}_2\mathit{X}]GaS_2$ depends on the salt-inclusion identity, the DFT-calculated electronic structures of *o*-$[Na_2Cl]GaS_2$ and *t*-$[Na_2Cl]GaS_2$ polymorphs are dominated by the GaS_2^- slabs. Experiments to test uranyl uptake in these layered structures showed that the salt-inclusion moiety can be exchanged with uranium, however, only with a concomitant structure decomposition.

Conflict of Interest

The authors declare that they have no conflicts of interest in this work.

Electronic supplementary information (ESI) available: Crystallographic data, EDS results, PXRD patterns, and UV-vis and IR spectra (PDF). Further details of the crystal structure investigations may be obtained from the joint CCDC/FIZ Karlsruhe online deposition service: https://www.ccdc.cam.ac.uk/ structures/ by quoting the deposition numbers CSD 2235684–2235689. For ESI and crystallographic data in CIF or other electronic format see DOI: 10.1039/ d0ce01524e

Acknowledgments

Research supported by the US Department of Energy, Office of Basic Energy Sciences, Division of Materials Sciences and Engineering under award DE-SC0018739.

References

(1) Dolbecq, A.; Dumas, E.; Mayer, C. R.; Mialane, P. Hybrid Organic-Inorganic Polyoxometalate Compounds: from Structural Diversity to Applications. *Chem. Rev.* **2010**, *110*, 6009-6048.

(2) Feng, J.; Zhang, H. Hybrid Materials Based on Lanthanide Organic Complexes: a Review. *Chem. Soc. Rev.* **2013**, *42*, 387-410.

(3) Gao, R.; Kodaimati, M. S.; Yan, D. Recent Advances in Persistent Luminescence Based on Molecular Hybrid Materials. *Chem. Soc. Rev.* **2021**, *50*, 5564-5589.

(4) Lebeau, B.; Innocenzi, P. Hybrid Materials for Optics and Photonics. *Chem. Soc. Rev.* **2011**, *40*, 886-906.

(5) Schubert, U. Cluster-Based Inorganic-Organic Hybrid Materials. *Chem. Soc. Rev.* **2011**, *40*, 575-582.

(6) Liras, M.; Barawi, M.; de la Peña O'Shea, V. A. Hybrid Materials Based on Conjugated Polymers and Inorganic Semiconductors as Photocatalysts: from Environmental to Energy Applications. *Chem. Soc. Rev.* **2019**, *48*, 5454-5487.

(7) Sanchez, C.; Belleville, P.; Popall, M.; Nicole, L. Applications of Advanced Hybrid Organic-Inorganic Nanomaterials: from Laboratory to Market. *Chem. Soc. Rev.* **2011**, *40*, 696-753.

(8) Wang, S.; Kang, Y.; Wang, L.; Zhang, H.; Wang, Y.; Wang, Y. Organic/Inorganic Hybrid Sensors: A Review. *Sens. Actuators, B* **2013**, *182*, 467-481.

(9) Draxl, C.; Nabok, D.; Hannewald, K. Organic/Inorganic Hybrid Materials: Challenges for *ab initio* Methodology. *Acc. Chem. Res.* **2014**, *47*, 3225-3232.

(10) Saparov, B.; Mitzi, D. B. Organic-Inorganic Perovskites: Structural Versatility for Functional Materials Design. *Chem. Rev.* **2016**, *116*, 4558-4596.

(11) Berry, J.; Buonassisi, T.; Egger, D. A.; Hodes, G.; Kronik, L.; Loo, Y. L.; Lubomirsky, I.; Marder, S. R.; Mastai, Y.; Miller, J. S.; Mitzi, D. B.; Paz, Y.; Rappe, A. M.; Riess, I.; Rybtchinski, B.; Stafsudd, O.; Stevanovic, V.; Toney, M. F.; Zitoun, D.; Kahn, A.; Ginley, D.; Cahen, D. Hybrid Organic-Inorganic Perovskites (HOIPs): Opportunities and Challenges. *Adv. Mater.* **2015**, *27*, 5102-5112.

(12) Brenner, T. M.; Egger, D. A.; Kronik, L.; Hodes, G.; Cahen, D. Hybrid Organic—Inorganic Perovskites: Low-Cost Semiconductors with Intriguing Charge-Transport Properties. *Nat. Rev. Mater.* **2016**, *1*, 15007.

(13) Li, W.; Wang, Z.; Deschler, F.; Gao, S.; Friend, R. H.; Cheetham, A. K. Chemically Diverse and Multifunctional Hybrid Organic–Inorganic Perovskites. *Nat. Rev. Mater.* **2017**, *2*, 16099.
(14) Zhou, H. C.; Kitagawa, S. Metal-Organic Frameworks (MOFs). *Chem. Soc. Rev.* **2014**, *43*, 5415-5418.
(15) Furukawa, H.; Cordova, K. E.; O'Keeffe, M.; Yaghi, O. M. The Chemistry and Applications of Metal-Organic Frameworks. *Science* **2013**, *341*, 1230444.
(16) Thorarinsdottir, A. E.; Harris, T. D. Metal-Organic Framework Magnets. *Chem. Rev.* **2020**, *120*, 8716-8789.
(17) Safaei, M.; Foroughi, M. M.; Ebrahimpoor, N.; Jahani, S.; Omidi, A.; Khatami, M. A Review on Metal-Organic Frameworks: Synthesis and Applications. *TrAC, Trends Anal. Chem.* **2019**, *118*, 401-425.
(18) Huang, Q.; Kartin, M.; Mo, X.; Hwu, S.-J. Synthesis of a New Class of Hybrid Solids *via* Salt Inclusion. *MRS Proceedings* **2002**, *755*, DD12.4.
(19) Hwu, S. J.; Ulutagay-Kartin, M.; Clayhold, J. A.; Mackay, R.; Wardojo, T. A.; O'Connor, C. J.; Krawiec, M. A New Class of Hybrid Materials *via* Salt Inclusion: Novel Copper(II) Arsenates $Na_5ACu_4(AsO_4)_4Cl_2$ (A = Rb, Cs) Composed of Alternating Covalent and Ionic Lattices. *J. Am. Chem. Soc.* **2002**, *124*, 12404-12405.
(20) Mo, X.; Ferguson, E.; Hwu, S. J. Salt-Inclusion Synthesis of Two New Polar Solids, $Ba_6Mn_4Si_{12}O_{34}Cl_3$ and $Ba_6Fe_5Si_{11}O_{34}Cl_3$. *Inorg. Chem.* **2005**, *44*, 3121-3126.
(21) Yakubovich, O. V.; Shvanskaya, L. V.; Kiriukhina, G. V.; Volkov, A. S.; Dimitrova, O. V.; Vasiliev, A. N. Hydrothermal Synthesis and a Composite Crystal Structure of $Na_6Cu_7BiO_4(PO_4)_4[Cl,(OH)]_3$ as a Candidate for Quantum Spin Liquid. *Inorg. Chem.* **2021**, *60*, 11450-11457.
(22) Choudhury, A.; Dorhout, P. K. Destruction of Noncentrosymmetry through Chalcogenide Salt Inclusion. *Inorg. Chem.* **2006**, *45*, 5245-5247.
(23) Dong, L.; Pan, S.; Wang, Y.; Yu, H.; Bian, Q.; Yang, Z.; Wu, H.; Zhang, M. $BaPbSi_2O_6{\cdot}BaSO_4$: the First Mixed Anionic Compound Synthesized *via* $BaSO_4$ Salt-Inclusion. *CrystEngComm* **2014**, *16*, 5993-5996.
(24) Juillerat, C. A.; Moore, E. E.; Morrison, G.; Smith, M. D.; Besmann, T.; zur Loye, H.-C. Versatile Uranyl Germanate Framework Hosting 12 Different Alkali Halide 1D Salt Inclusions. *Inorg. Chem.* **2018**, *57*, 11606-11615.
(25) Yue, Q. G.; Wei, W. B.; Chen, H.; Wu, X. T.; Lin, H.; Zhu, Q. L. Salt-Inclusion Chalcogenides: an Emerging Class of IR Nonlinear Optical Materials. *Dalton Trans.* **2020**, *49*, 14338-14343.
(26) Morrison, G.; zur Loye, H.-C. Expanding the Chemistry of Salt-Inclusion Materials: Utilizing the Titanyl Ion as a Structure Directing Agent for the Targeted Synthesis of Salt-Inclusion Titanium Silicates. *Cryst. Growth Des.* **2020**, *20*, 8071-8078.
(27) Carone, D.; Usman, M.; Klepov, V. V.; Smith, M. D.; Kocevski, V.; Besmann, T. M.; zur Loye, H.-C. New Germanate and Mixed Cobalt Germanate Salt Inclusion materials: $[(Rb_6F)(Rb_4F)][Ge_{14}O_{32}]$ and $[(Rb_6F)(Rb_{3.1}Co_{0.9}F_{0.96})][Co_{3.8}Ge_{10.2}O_{30}F_2]$. *CrystEngComm* **2020**, *22*, 8072-8080.
(28) Juillerat, C. A.; Klepov, V. V.; Smith, M. D.; zur Loye, H.-C. Targeted Crystal Growth of Uranium Gallophosphates *via* the Systematic Exploration of the UF_4–$GaPO_4$–ACl (A = Cs, Rb) Phase Space. *CrystEngComm* **2020**, *22*, 3020-3032.
(29) Volkov, S. N.; Charkin, D. O.; Arsentev, M. Y.; Aksenov, S. M.; Manelis, L. S.; Krzhizhanovskaya, M. G.; Sinelshchikova, O. Y.; Ugolkov, V. L.; Povolotskiy, A. V.;

Shilovskikh, V. V.; Antonov, A. A.; Bubnova, R. S. Where the Extraordinaries Meet: a Cascade of Isosymmetrical Superionic Phase Transitions and Negative Thermal Expansion in a Novel Silver Salt-Inclusion Borate Halide. *CrystEngComm* **2022**, *24*, 4174-4179.
(30) Klepov, V. V.; Juillerat, C. A.; Alekseev, E. V.; zur Loye, H.-C. Overstepping Löwenstein's Rule-A Route to Unique Aluminophosphate Frameworks with Three-Dimensional Salt-Inclusion and Ion-Exchange Properties. *Inorg. Chem.* **2019**, *58*, 724-736.
(31) Berseneva, A. A.; Masachchi, L. W.; Jacobsohn, L. G.; zur Loye, H.-C. Tunable Salt-Inclusion Chalcogenides for Ion-exchange, Photoluminescence, and Scintillation. *Chem. Mater.* **2023**, *35*, 1417-1431.
(32) Hiramatsu, H.; Yanagi, H.; Kamiya, T.; Ueda, K.; Hirano, M.; Hosono, H. Crystal Structures, Optoelectronic Properties, and Electronic Structures of Layered Oxychalcogenides *M*CuO*Ch* (*M* = Bi, La; *Ch* = S, Se, Te): Effects of Electronic Configurations of M^{3+} Ions. *Chem. Mater.* **2008**, *20*, 326-334.
(33) Zhou, X.; Malliakas, C. D.; Yakovenko, A. A.; Wilfong, B.; Wang, S. G.; Chen, Y.-S.; Yu, L.; Wen, J.; Balasubramanian, M.; Wang, H.-H.; Chung, D. Y.; Kanatzidis, M. G. Coherent Approach to Two-Dimensional Heterolayered Oxychalcogenides using Molten Hydroxides. *Nature Synthesis* **2022**, *1*, 729-737.
(34) Zhou, X.; Kolluru, V. S. C.; Xu, W.; Wang, L.; Chang, T.; Chen, Y. S.; Yu, L.; Wen, J.; Chan, M. K. Y.; Chung, D. Y.; Kanatzidis, M. G. Discovery of Chalcogenides Structures and Compositions using Mixed Fluxes. *Nature* **2022**, *612*, 72-77.
(35) Li, X.; Liang, F.; Liu, T.; Li, H. Na_2GaS_2Cl: a New Sodium-Rich Chalcohalide with Two-Dimensional $[GaS_2]_\infty$ Layers and Wide Interlayer Space. *Dalton Trans.* **2021**, *50*, 11167-11172.
(36) Eisenmann, B.; Hofmann, A. Crystal Structure of Potassium Phyllo-dithioindate(III), $KInS_2$. *Z. Kristallogr.* **1991**, *195*, 318-320.
(37) Saal, J. E.; Kirklin, S.; Aykol, M.; Meredig, B.; Wolverton, C. Materials Design and Discovery with High-Throughput Density Functional Theory: The Open Quantum Materials Database (OQMD). *JOM* **2013**, *65*, 1501-1509.
(38) Kirklin, S.; Saal, J. E.; Meredig, B.; Thompson, A.; Doak, J. W.; Aykol, M.; Rühl, S.; Wolverton, C. The Open Quantum Materials Database (OQMD): Assessing the Accuracy of DFT Formation Energies. *npj Comput. Mater.* **2015**, *1*, 15010.
(39) Adhikary, A.; Yaghoobnejad Asl, H.; Sandineni, P.; Balijapelly, S.; Mohapatra, S.; Khatua, S.; Konar, S.; Gerasimchuk, N.; Chernatynskiy, A. V.; Choudhury, A. Unusual Atmospheric Water Trapping and Water Induced Reversible Restacking of 2D Gallium Sulfide Layers in $NaGaS_2$ Formed by Supertetrahedral Building Unit. *Chem. Mater.* **2020**, *32*, 5589-5603.
(40) Klepov, V. V.; Berseneva, A. A.; Pace, K. A.; Kocevski, V.; Sun, M.; Qiu, P.; Wang, H.; Chen, F.; Besmann, T. M.; zur Loye, H. $NaGaS_2$: An Elusive Layered Compound with Dynamic Water Absorption and Wide-Ranging Ion-Exchange Properties. *Angew. Chem.* **2020**, *132*, 10928-10933.
(41) Manos, M. J.; Kanatzidis, M. G. Layered Metal Sulfides Capture Uranium from Seawater. *J. Am. Chem. Soc.* **2012**, *134*, 16441-16446.
(42) Manos, M. J.; Kanatzidis, M. G. Metal Sulfide Ion Exchangers: Superior Sorbents for the Capture of Toxic and Nuclear Waste-Related Metal Ions. *Chem. Sci.* **2016**, *7*, 4804-4824.
(43) Feng, M. L.; Sarma, D.; Qi, X. H.; Du, K. Z.; Huang, X. Y.; Kanatzidis, M. G. Efficient Removal and Recovery of Uranium by a Layered Organic-Inorganic Hybrid Thiostannate. *J. Am. Chem. Soc.* **2016**, *138*, 12578-12585.

(44) Berseneva, A. A.; Aziziha, M.; Schorne-Pinto, J.; Besmann, T. M.; zur Loye, H.-C. All-Inorganic Open-Framework Chalcogenides, $A_3Ga_5S_9{\cdot}xH_2O$ (*A* = Rb and Cs), Exhibiting Ultrafast Uranyl Remediation and Illustrating a Novel Post-Synthetic Preparation of Open-Framework Oxychalcogenides. *Chem. Mater.* **2022**, *34*, 8366-8378.